Acta Crystallographica Section D
Biological Crystallography
ISSN 1399-0047

Structure of the oligogalacturonate-specific KdgM porin

C. A. J. Hutter,[a]‡ R. Lehner,[a] Ch. Wirth,[a]§ G. Condemine,[b] C. Peneff[a] and T. Schirmer[a]*

[a]Focal Area of Structural Biology and Biophysics, Biozentrum, University of Basel, Klingelbergstrasse 70, CH-4056 Basel, Switzerland, and [b]Université de Lyon, F-69003; Université Lyon 1, F-69622; INSA-Lyon, Villeurbanne, F-69621; CNRS, UMR5240, Microbiologie Adaptation et Pathogénie, France

‡ Present address: Institut für Medizinische Mikrobiologie, University of Zürich, CH-8006 Zürich, Switzerland.
§ Present address: Institute of Biochemistry and Molecular Biology, University of Freiburg, D-79104 Freiburg, Germany.

Correspondence e-mail: tilman.schirmer@unibas.ch

Received 4 December 2013
Accepted 31 March 2014

PDB references: KdgM, 4fqe; K161S mutant, complex with $GA_{5,uns}$, 4pr7

The phytopathogenic Gram-negative bacterium *Dickeya dadantii* (*Erwinia chrysanthemi*) feeds on plant cell walls by secreting pectinases and utilizing the oligogalacturanate products. An outer membrane porin, KdgM, is indispensable for the uptake of these acidic oligosaccharides. Here, the crystal structure of KdgM determined to 1.9 Å resolution is presented. KdgM is folded into a regular 12-stranded antiparallel β-barrel with a circular cross-section defining a transmembrane pore with a minimal radius of 3.1 Å. Most of the loops that would face the cell exterior *in vivo* are disordered, but nevertheless mediate contact between densely packed membrane-like layers in the crystal. The channel is lined by two tracks of arginine residues facing each other across the pore, a feature that is conserved within the KdgM family and is likely to facilitate the diffusion of acidic oligosaccharides.

1. Introduction

Plant cells are protected by a rigid wall composed of three major carbohydrates: cellulose, hemicellulose and pectin. Pectin, in particular, provides rigidity to the cell wall by cross-linking cellulose and hemicellulose fibres. It is composed of α-1–4-linked galacturonate residues, some of which are methyl and/or acetyl esterified. Degradation of this polymer by pectinolytic enzymes is a devastating process for the plant, leading to cell necrosis and the so-called soft-rot disease that affects various plants of agricultural interest and causes significant economic losses every year (Hugouvieux-Cotte-Pattat *et al.*, 1996; Charkowski *et al.*, 2012). *Dickeya dadantii* (formerly named *Erwinia chrysanthemi*) is one of the phytopathogens responsible for this disease. The bacterium can process pectin by massively secreting pectinases to yield galacturonate oligomers (GA_n) of various lengths, mainly trimers and tetramers, that are used as a carbon source for growth (Condemine *et al.*, 1992; Kazemi-Pour *et al.*, 2004). The smaller oligomers can cross the outer membrane *via* the general OmpF porin, but in addition specific porins, KdgM and KdgN, have evolved to facilitate translocation, in particular of the larger GA_n oligomers (Blot *et al.*, 2002; Condemine & Ghazi, 2007). Their expression is up-regulated when GA_n is encountered in the environment.

In the periplasm, GA_n saccharides are subsequently further processed into shorter oligogalacturonates that can be transported through the inner membrane *via* theTogMNAB ABC transporter and the TogT symporter (Hugouvieux-Cotte-Pattat *et al.*, 2001) to finally enter the cytoplasm, where they are degraded to pyruvate and 3-phosphoglyceraldehyde, the final products that enter the general cellular metabolism to produce energy for the cell (Shevchik *et al.*, 1999).

Table 1
Data-collection and refinement statistics.

Values in parentheses are for the outer shell.

	Wild-type KdgM	$KdgM_{K161S}$–$GA_{5,uns}$
Data collection		
Beamline	X06DA, SLS	X06DA, SLS
Wavelength (Å)	1.008	1.008
Space group	$P2_1$	$P2_1$
Unit-cell parameters (Å, °)	a = 36.9, b = 59.7, c = 51.6, β = 106.8	a = 36.9, b = 59.7, c = 51.6, β = 106.5
Matthews coefficient (Å^3 Da^{-1})	2.2	2.2
Resolution (Å)	49.36–1.93 (2.03–1.93)	50.00–2.10 (2.21–2.10)
R_{merge}† (%)	7.3 (39.3)	7.8 (30.5)
Total reflections	61216 (8662)	34323 (2961)
Unique reflections	16187 (2329)	11990 (1419)
Completeness (%)	99.9 (99.9)	94.9 (77.5)
Multiplicity	3.8 (3.7)	2.9 (2.1)
Mean $I/\sigma(I)$	10.6 (3.4)	9.9 (2.3)
Refinement		
No. of atoms		
Protein	1411	1417
Detergent	129	135
Solvent	66	41
R_{work}/R_{free}‡ (%)	20.6/24.2	20.9/24.5
Average B factors (Å^2)		
Overall	30.0	33.3
Protein	27.8	32.4
Detergent	54.8	43.1
Solvent	31.6	31.5
R.m.s.d. from ideal		
Bond lengths (Å)	0.011	0.008
Bond angles (°)	1.507	1.222
Ramachandran plot (%)		
Favoured	96.9	98.7
Allowed	3.1	1.3
Outliers	0	0
PDB code	4fqe	4pr7

† $R_{merge} = \sum_{hkl}\sum_i |I_i(hkl) - \langle I(hkl)\rangle| / \sum_{hkl}\sum_i I_i(hkl)$, where $I_i(hkl)$ is the observed intensity for a reflection and $\langle I(hkl)\rangle$ is the average intensity obtained from multiple observations of symmetry-related reflections. ‡ $R = \sum_{hkl} ||F_{obs}| - |F_{calc}|| / \sum_{hkl} |F_{obs}|$; the test set for the R_{free} calculation comprised 5% of the data set.

The members of the KdgM porin family have the shortest sequence amongst the known outer membrane channels, with an average length of about 220 amino acids (molecular weight of about 25 kDa) for the mature protein. The KdgM family (Pfam family PF06178) currently comprises 1333 members distributed amongst 545 species, most of them Enterobacteriaceae spp., including plant and human pathogens such as uropathogenic or food-poisoning *Escherichia coli*, *Salmonella enterica*, *Yersinia pestis*, *Y. enterocolitica*, *Pectobacterium*, *Vibrio*, *Shigella* and *Pseudomonas* species. In most cases two and up to four homologous sequences are present in the genome, indicating a functional advantage for these bacteria to maintain several paralogues. For example, the two *D. dadantii* GA_n porins KdgM and KdgN are differentially expressed depending on the environmental conditions (Condemine & Ghazi, 2007).

Recently, the crystal structure of the *N*-acetylneuraminic acid-inducible NanC from *E. coli*, a member of the KdgM family, has been determined (Wirth *et al.*, 2009). The outer membrane protein is folded into a simple oval-shaped 12-stranded β-barrel that delimits a water-filled channel with an average radius of 3.3 Å. Conspicuously, the channel is lined by two tracks of basic residues that face each other across the pore and extend from the extracellular vestibule to the periplasm. Their potential role in the translocation of negatively charged oligosaccharides has been discussed.

KdgM from *D. dadantii* was the first member of the family to be functionally characterized (Blot *et al.*, 2002). It is essential for the transport of the longer ($n > 3$) GA_n pectin-degradation products. The virulence of the bacterium is significantly impaired in the knockout mutant, which makes this porin an interesting drug target. Ion translocation through KdgM was studied within artificial lipidic bilayers and showed an average conductance of 450 pS in 0.8 *M* KCl and anion selectivity (2.8-fold preference for chloride *versus* sodium translocation in a 0.8–0.1 *M* gradient). The ion current was blocked by the addition of trigalacturonate at millimolar concentrations. Here, we report an unusually densely packed crystal form of the integral outer membrane protein KdgM and describe its high-resolution structure.

2. Materials and methods

2.1. Protein expression, extraction and purification

KdgM was amplified from plasmid pKM2 (Blot *et al.*, 2002) with the primers KdgMHis+ (5′-GGGTTCGAATATAGGGAAAATACAATGAAG-3′) and KdgMHis− (5′-CCGAATTCAGTGGTGGTGGTGGTGGTGGAAGCTGTACTGCACGCCTAC-3′) to introduce a C-terminal His_6 tag. The amplified fragment was cloned into plasmid pGEM-T (Promega). A *Sac*I–*Eco*RI fragment was cut and introduced into the same sites of plasmid pKSM717 (Maneewannakul *et al.*, 1994) to create plasmid pKdgM-6His. To create single-point mutants of KdgM, site-directed mutagenesis was performed on plasmid pKM2 using the QuikChange kit (Stratagene). Mutagenized fragments were cut out with *Sph*I and *Eco*RI and introduced into plasmid pKSM717.

To produce the proteins, the plasmids were introduced into *E. coli* strain BL21(DE3)omp8/pLys [F− *ompT hsdSB gal dcm* Δ*lamB ompF*::Tn5 Δ*ompA* Δ*ompC* (DE3)] (Prilipov *et al.*, 1998). Transformants were grown in 3 l LB medium at 30°C. When the OD reached 1.5, IPTG was added to a concentration of 1 m*M* and the cells were grown for an additional 3 h. The bacteria were collected by centrifugation at 6000*g* for 10 min, resuspended in 10 m*M* Tris–HCl pH 8.0, 1 m*M* EDTA, treated with Benzonase (Merck, Darmstadt, Germany) and disrupted in a French press. Unbroken cells were eliminated by centrifugation at 6000*g* for 20 min and the membrane fraction was collected by centrifugation at 100 000*g* for 1 h.

To solubilize the inner membrane, membrane samples were diluted twofold with 50 m*M* Tris–HCl pH 8.0, 2%(*v*/*v*) lauroyl sarcosine (LS), homogenized and centrifuged for 1 h at ∼140 000*g*. Proteins were extracted from the outer membrane by stepwise solubilization with octyl-POE (Bachem). Outer membrane pellets were resuspended in 50 m*M* Tris–HCl pH 8.0 containing increasing concentrations of octyl-POE (Bachem) [0.5, 1, 2 and 3%(*v*/*v*)], homogenized and centri-

fuged for 30 min at ∼140 000*g*. The 2 and 3%(*v*/*v*) octyl-POE fractions contained the largest amounts of solubilized KdgM and were pooled.

Wild-type and mutant KdgM were purified using nickel-affinity chromatography with a 1 ml HisTrap HP column (GE Healthcare) equilibrated with 50 m*M* Tris–HCl pH 8.0, 0.6%(*v*/*v*) octyl-POE. The protein was eluted by applying an imidazole gradient up to 500 m*M*. KdgM-containing fractions were concentrated using an Amicon Ultra-4 centrifugal filter (Millipore) to a volume of 500 µl. To exchange the buffer, size-exclusion chromatography was applied. The protein sample was loaded onto a Superdex 200 10/300 GL column (Amersham Bioscience) equilibrated with 10 m*M* Tris–HCl pH 8.0, 100 m*M* NaCl, 0.5%(*v*/*v*) C_8E_4. Peak fractions were concentrated to 8 mg ml^{-1} and stored at 4°C for crystallization experiments.

2.2. Crystallization and soaking

A Phoenix robot (Art Robbins Instruments) was used for initial screening in 96-well plates (sitting-drop vapour-diffusion method) at 273 K. Crystals were obtained with the MPD Suite screen (Qiagen) only in the presence of digalacturonate (GA_2; Sigma) as an additive. Optimization was carried out in 24-well plates (hanging-drop and sitting-drop vapour-diffusion methods). Drops consisted of 1 µl protein solution at 2–6 mg ml^{-1} in 10 m*M* Tris–HCl pH 8.0, 100 m*M* NaCl, 0.5%(*v*/*v*) C_8E_4 and 1 µl reservoir solution. Plate-like crystals (0.3 × 0.3 mm) grew in a broad range of reservoir conditions: 100 m*M* MES pH 5.5–6.5 or 100 m*M* HEPES pH 7.0–7.5, 19–23% MPD, 36–72 m*M* GA_2. To obtain the structure of KdgM in complex with oligogalacturonate, crystals were soaked with 175 m*M* unsaturated $GA_{5,uns}$ (4,5-unsaturated pentagalacturonate; a gift from J. Benen, U. Wageningen) for 7 h in 100 m*M* MES pH 6.0, 25% MPD.

2.3. Data collection, processing, structure determination and refinement

Crystals were flash-frozen in liquid nitrogen without additional cryoprotectant and data were collected on beamline X06DA (PXIII) at the Swiss Light Source (SLS), Villigen, Switzerland using a MAR225 CCD detector. Diffraction data were indexed and integrated using *MOSFLM* (Leslie, 2006) and were scaled using *SCALA* (Evans, 2006). Phases were determined by molecular replacement using *Phaser* (McCoy *et al.*, 2007). *CHAINSAW* (Winn *et al.*, 2011) was used to obtain a modified model of NanC (PDB entry 2wjq; Wirth *et al.*, 2009) in which nonconserved residues were truncated to common atoms. Furthermore, three loops (119–128, 158–169 and 196–204) were removed from the search model. Refinement was carried out with *REFMAC*5 (Murshudov *et al.*, 2011) and manual model building in *Coot* (Emsley *et al.*, 2010). Waters were automatically placed with *ARP*/*wARP* (added for $F_o - F_c$ density > 4σ and removed for

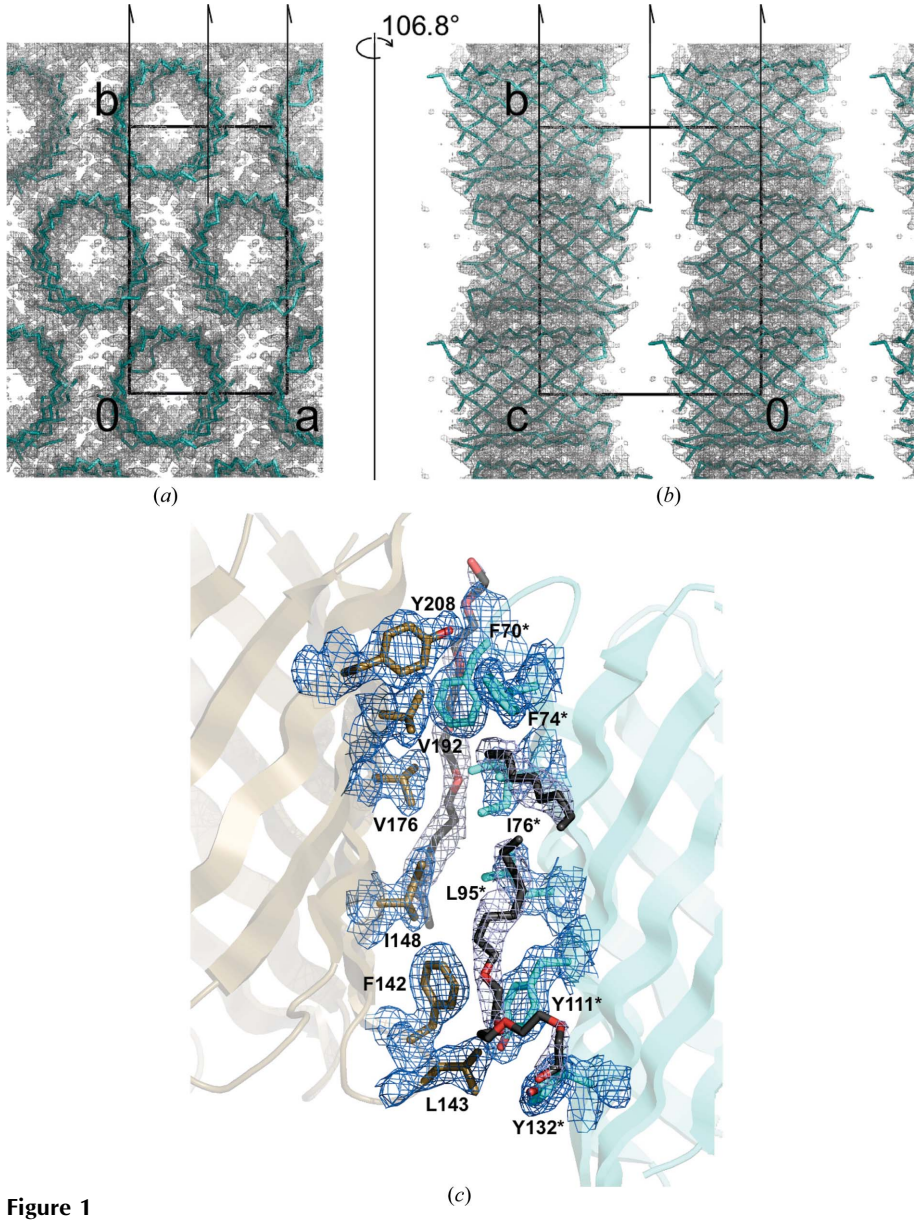

(*a*) (*b*) (*c*)

Figure 1
Crystal packing of KdgM. (*a*) View along the crystallographic *c* axis, (*b*) view along the *a* axis. The monoclinic unit cell and crystallographic 2_1 symmetry axes are shown in black. Superimposed on the $2F_o - F_c$ map (grey, contour level 1.2σ), the KdgM C$^\alpha$ traces are shown in cyan. (*c*) Close-up view of the major crystal contact between 2_1-related molecules within the *ab* plane. The *c* axis is vertical. The contact appears to mainly be defined by direct interactions between apolar side chains (yellow and cyan), but some detergent or lipid molecules (black) are also involved.

$F_o - F_c$ density $< 2.5\sigma$). Stereochemical validation of the structures was performed using the *MolProbity* server (Chen *et al.*, 2010). The KdgM pore dimensions were quantified and the pore lumen was visualized with the program *HOLE* (Smart *et al.*, 1996).

3. Results and discussion

3.1. Structure determination

Wild-type KdgM, $KdgM_{K124S}$ and $KdgM_{K161S}$ including the native signal sequence and a C-terminal His_6 tag were overexpressed in *E. coli*. The point mutations were chosen following the surface-entropy reduction strategy (Derewenda, 2004) to potentially facilitate subsequent crystallization. For this, a KdgM homology model was generated on the basis of the structure of NanC porin to predict surface-exposed lysine and glutamate residues. Four nonconserved lysine (Lys124, Lys130, Lys156 and Lys161) as well as two glutamate residues (Glu199 and Glu203) were identified to probably reside in external loops that often mediate crystal contacts in porins. The homology model also predicted solvent exposure of the C-terminus, justifying the addition of a C-terminal tag. The

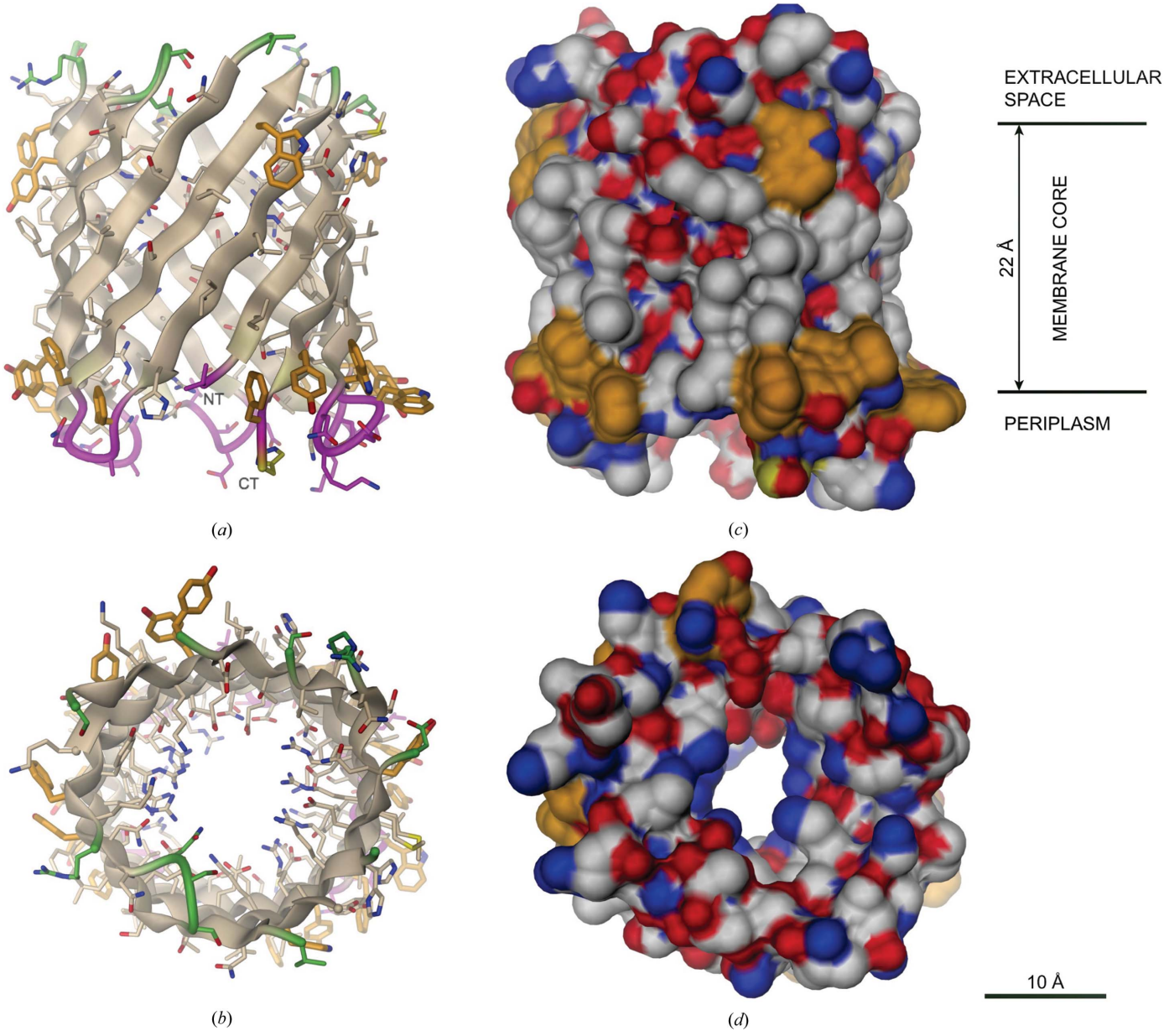

Figure 2
Crystal structure of KdgM. (*a*, *b*) Cartoon representation showing the transmembrane β-strand (ribbons), the extracellular loops (green tubes) and the periplasmic turns (magenta tubes) of the 12-stranded β-barrel. In addition, all side chains are shown in full. Aromatic side chains of the two girdles are coloured gold. NT and CT indicate the chain termini. View from within the membrane (*a*) and from the cell exterior (*b*). (*c*, *d*) The same views as in (*a*) and (*b*) but in molecular-surface representation. Horizontal lines indicate the approximate boundaries of the outer-membrane hydrophobic core as defined by the aromatic girdles (gold).

proteins were extracted from the outer membrane with octyl-POE and further purified *via* affinity chromatography.

A final size-exclusion chromatography step was performed to exchange detergent prior to crystallization. Many detergents, such as *N*,*N*-dimethyldodecylamine *N*-oxide (LDAO) and polyethylene glycol monooctyl ethers (C_8E_4 and C_8E_5), as well as sugar-based detergents such as octyl or nonyl glucoside, were tested for crystallization of wild-type KdgM. Crystals appeared in many conditions, especially in C_8E_4, C_8E_5 and octylglucoside. Notably, all successful detergents had eight-carbon acyl chains. The surface-entropy-reduced mutants were tested for crystallization in a second phase. Clearly, compared with the results for wild-type KdgM, even more hits were obtained. For example, $KdgM_{K124S}$ in LDAO yielded crystalline objects in 24 of the 384 tested conditions. Nine of the successful conditions gave harvestable crystals, although the crystals only diffracted to low resolution.

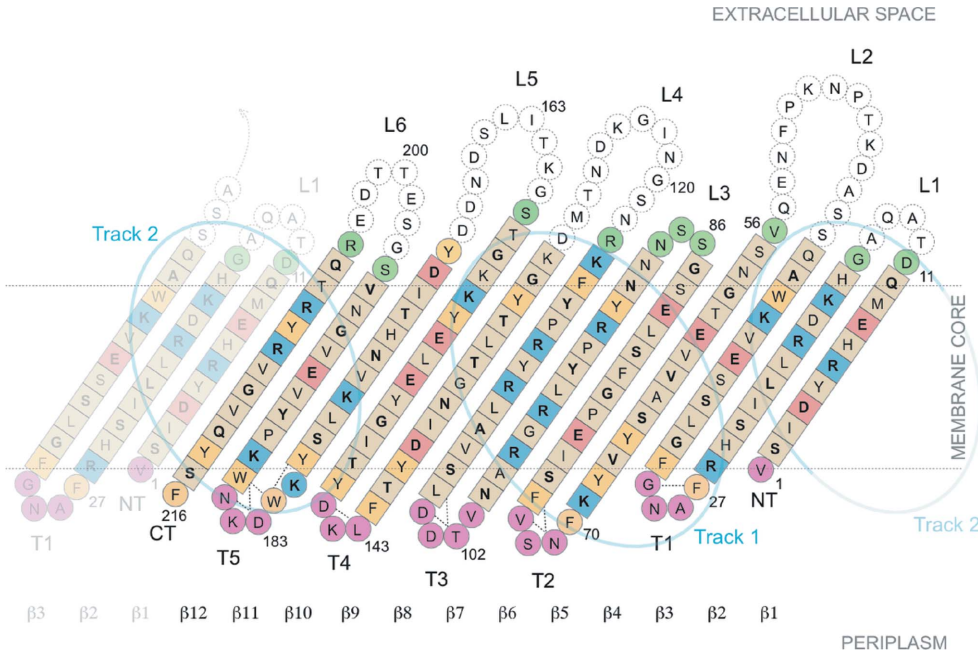

Figure 3
Topology diagram of KdgM. The first three β-strands are repeated to indicate interactions closing up the barrel. Circled residues belong to loop regions and residues in squares belong to β-strands. Residues indicated in bold have their side chain pointing towards the pore interior, with basic residues coloured blue (forming tracks 1 and 2) and acidic residues red. Otherwise, the same colour code is used as in Fig. 2. Extracellular loops without defined structure are shown in dashed circles. Hydrogen bonds in turns are shown as black dashed lines.

A breakthrough was achieved with the addition of digalacturonate (GA_2), a substrate of KdgM. Well diffracting plate-like crystals belonging to space group $P2_1$ were obtained for both wild-type KdgM and the K161S mutant. Data-collection statistics are given in Table 1. The structure was solved by molecular replacement using a truncated model of the homologous NanC porin (PDB entry 2wjq; Wirth *et al.*, 2009). The quality of the electron-density map allowed the tracing of 80% of the polypeptide chain; the segments 12–15, 42–55, 118–129, 160–169 and 197–203 were not traced. Subsequent refinement yielded a wild-type KdgM model with final R and R_{free} values of 20.6 and 24.2%, respectively (Table 1).

3.2. Crystal packing

Fig. 1 shows that monomeric KdgM porin molecules are arranged into a densely packed layer in the *ab* plane of the monoclinic crystal. The layer is stabilized by lateral contacts between the porin β-barrels, mainly involving direct van der Waals contacts between their apolar surfaces. In addition, elongated density features, which have been modelled as detergent acyl chains, are observed as part of the contacts. Details of the major crystal contacts can be seen in Fig. 1(*c*). Neighbouring barrels in the crystal layer are oriented up and down (according to the crystallographic 2_1 axes parallel to *b*). Note that such an arrangement is artificial and will not occur in the native outer membrane.

The protein layers are stacked on top of each other according to the *c* translation symmetry. Since the pore axis of the barrel is oriented approximately perpendicular to the *ab* plane, pores of adjacent layers are roughly aligned, resulting in the appearance of water-filled channels that run through the entire crystal (Figs. 1*a* and 1*b*). The use of such crystals for the development of highly precise filtering devices appears to be attractive.

Paradoxically, there is virtually no electron density between the layers. The closest distance (5 Å) is observed between Arg204 and Lys130* from an antiparallel molecule of the adjacent layer. Layer contact must be mediated by structurally heterogenous elements. In fact, large segments of the extracellular loops are not defined by density (see below) but would be large enough to establish inter-layer contacts. Thus, the pile-up of presumably rather rigid and well ordered layers also appears to mediate long-range crystalline order in the direction of the layer normal.

3.3. Overall structure

KdgM is folded into a 12-stranded antiparallel β-barrel encompassing a transmembrane pore (Fig. 2). Its structure is similar to that of NanC (Wirth *et al.*, 2009), with which it shares 24% sequence identity. 172 C^{α} positions superimpose with an r.m.s.d. of 1.4 Å. The cross-section of the barrel is almost circular, with dimensions of about 23 × 25 Å as defined by the

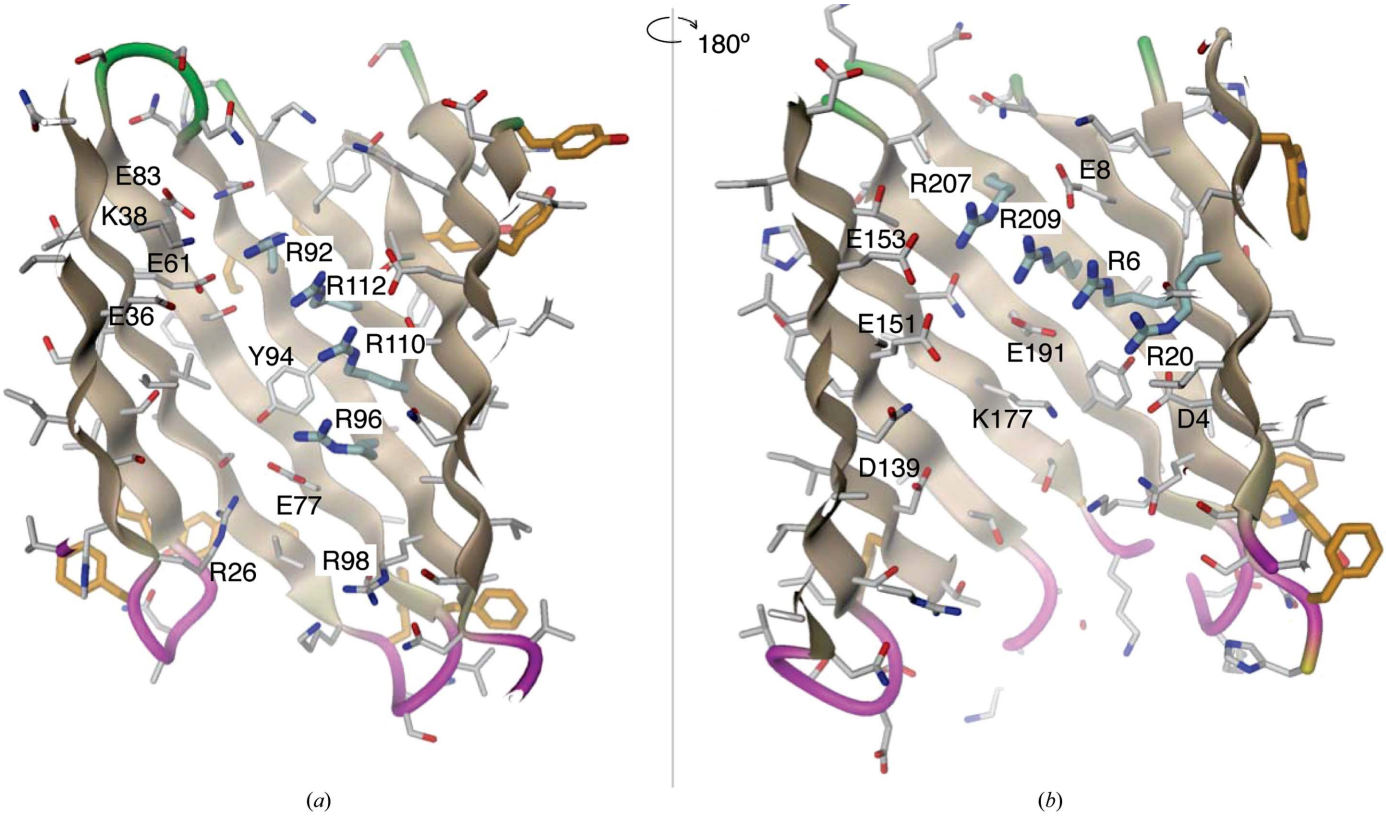

Figure 4
Pore architecture. (*a*, *b*) Cut-open views of the pore related by a 180° rotation about the pore axis. All side chains are shown and charged or aromatic residues are labelled. The arginines of the two tracks are emphasized by larger bond width. (*a*) Track 1, (*b*) track 2. Two side-chain conformations have been modelled for Arg112, of which only one is shown. (*c*) Pore lumen as visualized by *HOLE* with charged side chains at the most constricted region (r = 3.1 Å) shown in full.

backbone, whereas NanC has a more elliptical cross-section (20 × 26 Å). The β-strands are connected by short turns on the periplasmic side, which is a typical feature of porins. Strikingly, all loops on the extracellular side, except for the short L3 loop, are not defined by electron density, although they are present and have not been cleaved by proteolysis as shown by SDS–PAGE and mass spectrometry. The same was observed for the surface-entropy reduction mutant K161S that affects a residue in one of the disordered loops (data not shown). Disorder of extracellular loops has been observed before for porins, for example for OmpG (Subbarao & van den Berg, 2006).

The β-strands are amphiphilic, as expected for a β-barrel that encompasses an aqueous pore and is incorporated in the membrane. The topology diagram (Fig. 3) demonstrates that barrel residues facing the outside are hydrophobic, with few exceptions, whereas the residues pointing inwards are mainly hydrophilic and are often charged. The apolar outer surface of the β-barrel (Fig. 2) would face the core of the outer membrane *in vivo*. Two belts composed of aromatic residues delimit this part of the surface (Fig. 2), a feature that is typical of membrane proteins.

3.4. Pore structure

The KdgM pore is lined by a large number of charged residues (Figs. 2 and 4). Conspicuously, there are two clusters of arginine side chains that face each other across the pore. Each of the clusters forms a right-handed helical track at the pore lining (track 1 and track 2), as can been seen in the side

views in Figs. 4(*a*) and 4(*b*). The two tracks are flanked at the pore entrance and outlet by eight lysine residues (by Lys69, Lys116 and Lys155 and by Lys18, Lys38, Lys177, Lys181 and Lys187, respectively). Additionally, 11 carboxylic side chains (Asp4, Glu8, Glu36, Glu61, Glu77, Glu83, Asp139, Glu151, Glu153, Asp171 and Glu191) are part of the pore lining, with only four of them being engaged in salt bridges with track residues. The quadrupolar arrangement of track 1, Glu151/Glu153, track 2 and Glu36/Glu61 define the narrowest part of the channel (Fig. 4*c*), with a radius of 3.1 Å as defined by *HOLE* (Smart *et al.*, 1996).

The peculiar accumulation and segregation of charged residues at the KdgM pore lining has been observed before in the crystal structure of NanC (Wirth *et al.*, 2009). At the time, structural modelling had already predicted the conservation of this electrostatic feature in KdgM and also in other members of the family. The sequence alignment shown in Fig. 5 shows that five of the nine track residues are conserved (KdgM residues 6, 20, 209, 110 and 112) in NanC and one (residue 96) is mutated to a lysine. This contrasts with a 25% conservation of the other charged pore residues and suggests an outstanding functional role for the tracks. Unlike in the NanC porin, there are only two aromatic residues at the pore lining. These are Tyr94 and Tyr189, which are situated just underneath tracks 1 and 2, respectively, and appear to support the extended conformation of the arginines as in NanC. Also of interest is the conservation of Gly79 and Gly211 (Fig. 5) which appears to be linked to the conservation of the aforementioned tyrosines, since the missing side chains permit the packing of Tyr94 and Tyr189 with the inner surface of the barrel.

Intriguingly, four largely conserved proline residues (Pro78, Pro93, Pro113 and Pro188) are found as part of transmembrane β-strands (Figs. 3 and 5). Despite (i) the constraint imposed by the circular side chain and the resulting deviation of the φ main-chain torsion angle ($\varphi = -66 \pm 5^{\circ}$) from the extended conformation and (ii) the missing hydrogen-bond donor functionality of the main-chain amide, these proline residues are surprisingly well accomodated in the barrel fold. Conspicuously, all four residues have their side chains protruding outside, where they would be exposed to the membrane core *in vivo*. Thus, proline residues appear to qualify well for the outer surface of transmembrane β-strands.

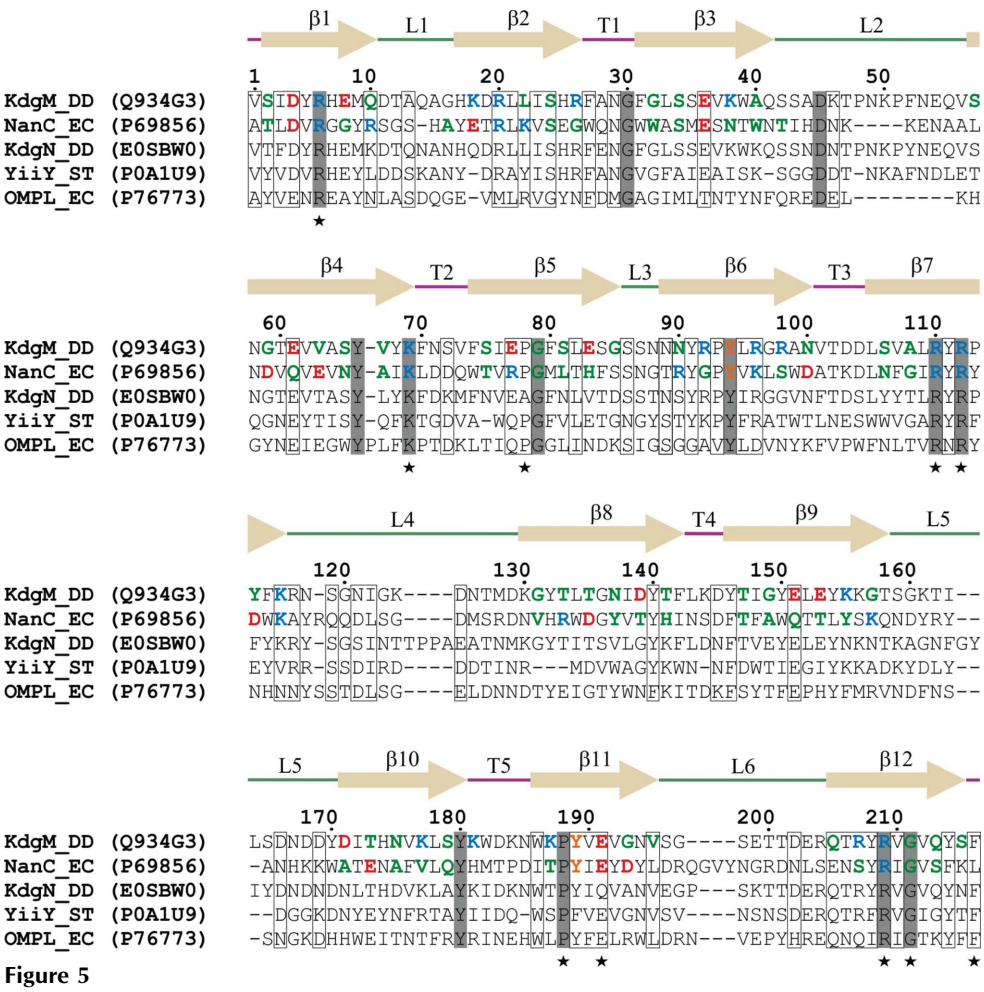

Figure 5
Sequence alignment of selected KdgM family members. The accession codes for the proteins are shown in parentheses. DD, EC and ST stand for *D. dadantii*, *E. coli* and *Salmonella typhi*, respectively. The alignment was generated by *ClustalW*2 and has been modified slightly to be consistent with the structure-based alignment of KdgM with NanC. Fully conserved residues are shown with a grey background; semi-conserved residues are boxed. Secondary structure and residue numbers of KdgM are depicted at the top. KdgM and NanC residues that are part of the pore lining are shown in colour (blue, basic residues; red, acidic residues; green, pore residues; orange, tyrosine residues). Stars mark highly conserved residues within the KdgM family (Pfam family PF06178) according to the HMM logo.

3.5. Substrate complex and translocation mechanism

To gain insight into the translocation mechanism of the natural substrate, co-crystallization experiments were performed with $KdgM_{K161S}$ and oligogalacturonides (up to 30 m*M*) of different lengths dissolved in 10 m*M* Tris–HCl pH 6.0, but no diffracting crystals were obtained. Therefore, a native $KdgM_{K161S}$ crystal was soaked in 175 m*M* $GA_{5,uns}$ at pH 6.0 and the structure was determined to 2.1 Å resolution. The complex structure superimposes closely with the native structure. The same disorder is seen in the extracellular loops as in the native structure. Fig. 6(*a*) shows that there is weak fragmented residual density along the axis of the pore, but this did not

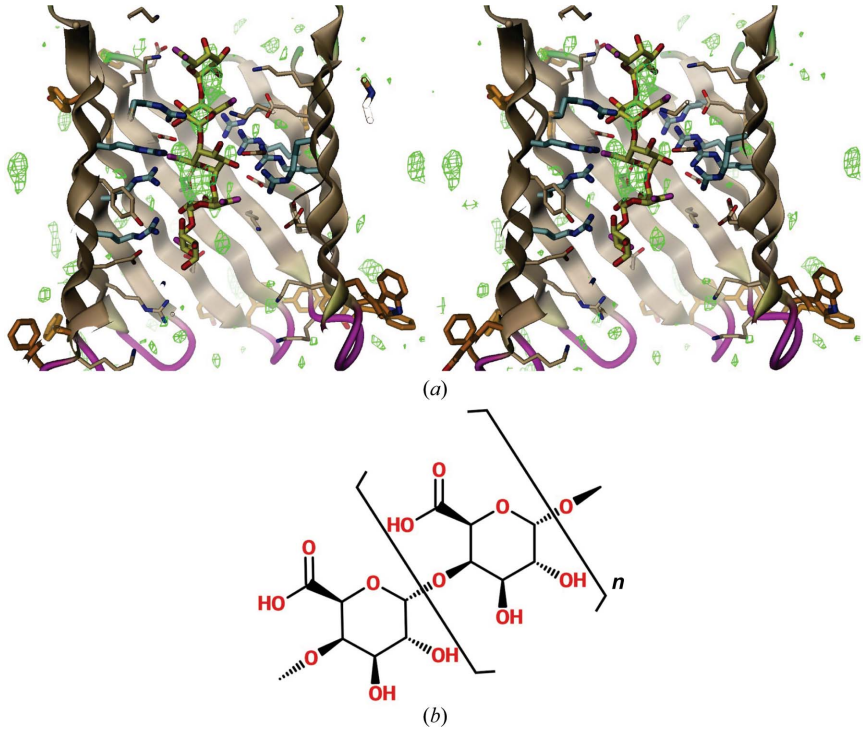

Figure 6
(*a*) Model of GA_5 as bound to KdgM (stereoview). A GA_5 oligosaccharide (yellow C atoms) with approximate 2_1 symmetry [repetitive glycosidic torsion angles (φ, ψ) = 120, 150°] has been positioned manually in the KdgM channel such that its carboxylate groups (magenta O atoms) form ionic interactions with both positively charged tracks. The model is included in PDB entry 4pr7. Also shown is the residual $F_o - F_c$ density (green, contoured at 3.0σ) obtained after soaking a crystal in 175 m*M* $GA_{5,uns}$. (*b*) Chemical structure of oligogalacturonate (GA_n).

warrant building a model for a bound saccharide. Considering the relatively large pore lumen and the weak, *i.e.* millimolar, affinity previously determined by ion-flow blockage (Blot *et al.*, 2002), this is perhaps not surprising. It is quite conceivable that the path of the oligosaccharide through the pore is not unique and that there are a multitude of binding modes.

Oligogalacturonate (Fig. 6*b*) in a conformation with approximate 2_1 symmetry [repetitive glycosidic torsion angles (φ, ψ) = 120, 150°; Seyedarabi *et al.*, 2010] can easily be accommodated within the channel (Fig. 6*a*). In this conformation the carboxylic side chains of consecutive residues point in opposite directions and are well suited for interacting with the two basic tracks, as has also been suggested based on molecular dynamics for the binding of *N*-acetylneuraminic acid oligomers to the NanC pore (Wirth *et al.*, 2009). It can be expected that as found for maltoporin (Dutzler *et al.*, 1996) and other facilitated diffusion channels (Moraes *et al.*, 2007), the negatively charged oligosaccharide will not experience large energy barriers during translocation, since at any given time the substrate can engage in a multitude of ionic and hydrogen-bonding interactions. Further functional studies in combination with site-directed mutagenesis are now needed to test the translocation mechanism.

We would like to thank the team at the Swiss Light Source, Villigen, Switzerland for their excellent support. This work was supported by Swiss National Science Foundation grant No. 3100AO-105587 to TS.

References

Blot, N., Berrier, C., Hugouvieux-Cotte-Pattat, N., Ghazi, A. & Condemine, G. (2002). *J. Biol. Chem.* **277**, 7936–7944.
Charkowski, A. *et al.* (2012). *Annu. Rev. Phytopathol.* **50**, 425–449.
Chen, V. B., Arendall, W. B., Headd, J. J., Keedy, D. A., Immormino, R. M., Kapral, G. J., Murray, L. W., Richardson, J. S. & Richardson, D. C. (2010). *Acta Cryst.* D**66**, 12–21.
Condemine, G., Dorel, C., Hugouvieux-Cotte-Pattat, N. & Robert-Baudouy, J. (1992). *Mol. Microbiol.* **6**, 3199–3211.
Condemine, G. & Ghazi, A. (2007). *J. Bacteriol.* **189**, 5955–5962.
Derewenda, Z. S. (2004). *Structure*, **12**, 529–535.
Dutzler, R., Wang, Y.-F., Rizkallah, B., Rosenbusch, J. P. & Schirmer, T. (1996). *Structure*, **4**, 127–134.
Emsley, P., Lohkamp, B., Scott, W. G. & Cowtan, K. (2010). *Acta Cryst.* D**66**, 486–501.
Evans, P. (2006). *Acta Cryst.* D**62**, 72–82.
Hugouvieux-Cotte-Pattat, N., Blot, N. & Reverchon, S. (2001). *Mol. Microbiol.* **41**, 1113–1123.
Hugouvieux-Cotte-Pattat, N., Condemine, G., Nasser, W. & Reverchon, S. (1996). *Annu. Rev. Microbiol.* **50**, 213–257.
Kazemi-Pour, N., Condemine, G. & Hugouvieux-Cotte-Pattat, N. (2004). *Proteomics*, **4**, 3177–3186.
Leslie, A. G. W. (2006). *Acta Cryst.* D**62**, 48–57.
Maneewannakul, S., Maneewannakul, K. & Ippen-Ihler, K. (1994). *Plasmid*, **31**, 300–307.
McCoy, A. J., Grosse-Kunstleve, R. W., Adams, P. D., Winn, M. D., Storoni, L. C. & Read, R. J. (2007). *J. Appl. Cryst.* **40**, 658–674.
Moraes, T. F., Bains, M., Hancock, R. E. W. & Strynadka, N. C. J. (2007). *Nature Struct. Mol. Biol.* **14**, 85–87.
Murshudov, G. N., Skubák, P., Lebedev, A. A., Pannu, N. S., Steiner, R. A., Nicholls, R. A., Winn, M. D., Long, F. & Vagin, A. A. (2011). *Acta Cryst.* D**67**, 355–367.

Prilipov, A., Phale, P. S., Van Gelder, P., Rosenbusch, J. P. & Koebnik, R. (1998). *FEMS Microbiol. Lett.* **163**, 65–72.
Seyedarabi, A., To, T. T., Ali, S., Hussain, S., Fries, M., Madsen, R., Clausen, M. H., Teixteira, S., Brocklehurst, K. & Pickersgill, R. W. (2010). *Biochemistry*, **49**, 539–546.
Shevchik, V. E., Condemine, G., Robert-Baudouy, J. & Hugouvieux-Cotte-Pattat, N. (1999). *J. Bacteriol.* **181**, 3912–3919.
Smart, O. S., Neduvelil, J. G., Wang, X., Wallace, B. A. & Sansom, M. S. (1996). *J. Mol. Graph.* **14**, 354–360.
Subbarao, G. V. & van den Berg, B. (2006). *J. Mol. Biol.* **360**, 750–759.
Winn, M. D. *et al.* (2011). *Acta Cryst.* D**67**, 235–242.
Wirth, C., Condemine, G., Boiteux, C., Bernèche, S., Schirmer, T. & Peneff, C. M. (2009). *J. Mol. Biol.* **394**, 718–731.